Environmental Fluid Mechanics (2026) 26:17
https://doi.org/10.1007/s10652-026-10080-6

ORIGINAL ARTICLE

A CFD modelling study of atmospheric particulate matter dry deposition on electrical insulators

Nicola Luciano[1] · Domenico Toscano[1] · Alessandra Balzarini[1] · Guido Pirovano[1]

Received: 27 November 2025 / Accepted: 7 March 2026 / Published online: 16 March 2026

Abstract
Surface contamination of overhead power line insulators poses a significant risk to the reliability and operational continuity of electrical networks. This study develops and validates a three-dimensional Computational Fluid Dynamics (CFD) model to investigate dry aerosol deposition on a chain of U120B glass insulators, with a focus on the underlying aerodynamic mechanisms. The model employs an Eulerian-Lagrangian approach to resolve the coupled dynamics of turbulent airflow and particle transport, incorporating molecular and turbulent diffusion, inertial and gravitational effects, and a detailed representation of the insulator geometry. Validation against established experimental datasets confirms the model's ability to accurately predict deposition velocities across a broad spectrum of particle sizes and flow regimes. Application of the framework reveals that local flow structures, such as recirculation zones, boundary layer separation, and adverse pressure gradients, influence the pollutants deposition spatial distribution, with different deposition velocities on the top and bottom surfaces of the insulators. The analysis demonstrates that wind speed and particle size critically influence deposition efficiency, with non-monotonic behaviours emerging under specific conditions. These findings provide a predictive, physics-based foundation for optimizing insulator design and maintenance strategies, supporting enhanced resilience of power systems to environmental contamination.

Keywords Power line insulators · Insulator contamination · Aerosol-surface interactions · Aerosol dry deposition · Turbulent particle transport · Deposition velocity · Atmospheric particulate matter (PM) · Power grid resilience · Risk assessment · Computational fluid dynamics (CFD)

✉ Nicola Luciano
nicola.luciano@rse-web.it

[1] Ricerca sul Sistema Energetico - RSE S.p.A, Via R. Rubattino 54, 20134 Milano, Italy

1 Introduction

The contamination of electrical insulators on overhead power lines, resulting from the deposition of atmospheric particulate matter (PM), represents a significant threat to the reliability and resilience of power systems [1, 2]. Contamination accumulation can lead to altered surface properties [3]; while polluted insulators maintain their dielectric properties in dry conditions, the presence of atmospheric moisture from sources such as dew, fog, or rain can dissolve accumulated hygroscopic particles on their surfaces [4]. This process leads to the formation of a conductive layer that significantly increases surface conductivity, potentially causing surface discharges, flashover events, and consequent service interruptions with substantial economic repercussions [2, 5].

The accumulation of pollutants on an insulator is a complex process governed by the interplay of multiple physical phenomena and influencing factors. The mechanisms driving dry deposition include sedimentation, inertial impaction, turbulent impaction, interception [6], with drag force, gravity, and Saffman's lift playing a relevant role [3, 7, 8]. The efficiency of these mechanisms is intrinsically linked to the physical properties of the particles, such as their size, density, and aerodynamic characteristics, as well as the local flow field characteristics [9, 10]. Consequently, the surface contamination of an insulator is strongly dependent on wind velocity and particle size distribution of the aerosol, given the structural design [10, 11]. Moreover, particle deposition may be affected by the insulator surface properties [12].

From a fluid dynamics perspective, the complex geometry of insulators, characterized by sheds, ribs, and caps, induces a highly intricate flow field [10, 13]. This field features regions of flow acceleration, separation, and the formation of vortices, which fundamentally dictate particle trajectories and deposition patterns [3]. It is well-documented that contamination is distributed non-uniformly across the insulator surface [3, 10, 14]. A recurrent observation is the higher accumulation of pollutants on the leeward side, which is attributed to the formation of low-velocity recirculation zones where particles have a longer residence time and can settle out of the flow [3, 10]. This phenomenon is driven by the combined action of a reverse pressure gradient and flow stagnation effects on the insulator's leeward surface [3]. However, the deposition pattern is highly dependent on the insulator's profile; for instance, some studies on rod-type cantilever insulators have reported a greater degree of contamination on the windward side [14]. The distribution between the top and bottom surfaces is also profile-dependent, with disc-shaped insulators typically showing higher contamination on the bottom surface, whereas shed-shaped insulators exhibit the opposite trend [10]. A critical feature of the airflow is the boundary layer separation phenomenon [3].

Wind velocity and particle properties are paramount in determining the rate and distribution of contamination. An increase in wind speed generally intensifies the deposition process and enhances the non-uniformity of the contaminant layer [3, 10]. The deposition efficiency is a function of both particle diameter and wind velocity and may exhibit non-monotonic behaviors, as in [3, 11]. The influence of particle size is particularly pronounced for coarse particles (d_p>10 μm) [15]. Conversely, for sub-micron particles, the collision coefficient is typically low and shows little variation with wind speed [11]. A comprehensive model for PM deposition flux identifies it as a function of several parameters, including the Reynolds number (Re), the particle diameter, and the particle density [13].

To investigate these phenomena, natural contamination tests, controlled laboratory experiments in wind tunnels, and advanced numerical simulations have been used [3]. Wind tunnel tests, in particular, provide a controlled environment to systematically study the influence of variables such as wind speed and particle size on contamination patterns [10]. In parallel, Computational Fluid Dynamics (CFD) has become an indispensable tool for analyzing the complex airflow and particle transport around insulators [11, 13]. Wind-tunnel-validated CFD indicates that shed geometry governs retention patterns, with configuration effects strengthening as wind speed increases [16]. Under HVDC, coupling flow/charging with CFD reproduces along-string non-uniform deposition and field-intensity-dependent accumulation [17]. Methodologies such as Eulerian multiphase models [4, 10] and Lagrangian particle tracking [13] are commonly employed to simulate the deposition process. A 2-D COMSOL setup is used as a CFD prototype to explore wind-driven adhesion patterns [18]. RANS approaches with 2-equation turbulence models are often chosen for their capacity to combine relatively low computational effort and ability to accurately handle flows with high strain rates and significant streamline curvature, which are characteristic of the flow around insulators [4, 6, 11, 13]. The strong agreement observed between CFD predictions and experimental results has solidified the role of numerical simulation as a valid and efficient approach for evaluating the surface contamination of different insulator designs and understanding the underlying physical mechanisms [3, 10].

This research aims to develop an advanced CFD-based modeling framework to systematically analyze the aerodynamic mechanisms governing surface contamination on outdoor insulators. By focusing on fluid dynamics, this study seeks to isolate the flow and particles properties effects on particle deposition, providing new insights that can inform the design of insulators optimized for reduced contamination buildup in diverse environmental conditions. Through a combination of numerical simulations and experimental validation, this work will contribute to the development of more accurate predictive models, ultimately supporting improved maintenance strategies and enhanced reliability of electrical power systems. The experimental validation has been conducted against a well-established atmospheric aerosol deposition dataset, while publicly available experimental data of particle deposition on insulators are not currently available, to the best of the authors' knowledge.

The remainder of this work is organized as follows. In Sect. 2 the implemented CFD model for the insulator surface contamination is described and validated against particle deposition experimental data. Investigated conditions are presented, including the modelled geometry and flow conditions imposed, coherent with aerosol and meteorological experimental data obtained from dedicated measurement campaigns. The results of the CFD model application to the investigated conditions are presented and discussed in Sect. 3. Lastly, Sect. 4 is dedicated to conclusions and future perspectives of this work.

2 Materials and methods

2.1 Numerical model of the insulators surface contamination

Electrical insulators surface contamination is a complex process, resulting from the combination of several interacting phenomena, such as the turbulent airflow around the insulators, the particles transport and deposition, wall-flow interaction. In order to properly account for this complexity, a 3D Computational Fluid Dynamics model has been developed in ANSYS Fluent [19] and applied to simulate pollutant deposition on the surface of a full-scale IEC-standard U120B type electrical glass insulator [20].

The particles transport in atmospheric air can be framed as a multiphase flow, with air and pollutants in gas and solid phase, respectively. In this context, the multiphase flow is considered to be a dispersed flow in dilute conditions [21], with air being the continuous phase and pollutant particles being the dispersed phase. Mass transfer between the two phases is not modelled in this study, surface contamination is assumed to be due to dry deposition exclusively, and air is considered to be in dry conditions. An Eulerian-Lagrangian approach has been implemented [22], with dedicated interacting models for each of the two phases. Airflow is modelled within an Eulerian framework for turbulent flows, whereas solid particles are modelled with a Lagrangian method. The choice of an Eulerian-Lagrangian framework over Eulerian-Eulerian or empirical models is dictated by the requirement for high-fidelity resolution of deposition patterns on complex geometries. While Eulerian-Eulerian models treat the particulate phase as a continuum, the Eulerian-Lagrange approach allows for the direct integration of individual forces on discrete trajectories. This avoids the inherent difficulties of Eulerian-Eulerian models in defining accurate near-wall boundary conditions for particle concentration, which often necessitate complex closures or kinetic theory treatments [23]. By tracking discrete trajectories, the Eulerian-Lagrangian framework provides a more direct representation of the discrete nature of the deposition process. Furthermore, while empirical correlations, e.g., Lai & Nazaroff [24], are computationally efficient, they are typically derived from canonical flows and lack the versatility to account for the multi-element geometric features of electrical insulators. Ambient air is modelled at constant density and viscosity, as the incompressible flow hypothesis is supported by the low air velocity [3]; a uniform temperature field is modelled. The airflow has turbulent behaviour and RANS approach is applied for turbulence modelling, with Shear-Stress Transport k-ω model used for turbulence closure, proven to be particularly capable to successfully blend correct wall treatment with proper modelling of the bulk flow [25]. The governing equations of the flow around the insulator are the continuity equation, momentum equation and turbulence closure equations, all used in their standard formulation in Fluent [26]. Energy transfer, chemical reactions and electrical effects are assumed to be negligible within the scope of this study, which focuses on the fluid dynamics contribution on the dry deposition process. Pollutant particles are modelled as disperse phase with a Lagrangian approach, assumed to be inert spherical particles characterized by their constant density and uniform diameter. Applying the dilute flow hypothesis, the particle-particle interactions and the influence of the disperse phase on the fluid phase are assumed to be negligible [23]. The particle trajectory is obtained integrating the force balance on the particle written in a Lagrangian reference frame, Eq. 1:

$$m_p \frac{d\boldsymbol{u_p}}{dt} = m_p \frac{\boldsymbol{u} - \boldsymbol{u_p}}{\tau_r} + m_p \frac{\boldsymbol{g}\,(\rho_p - \rho)}{\rho_p} + \boldsymbol{F} \tag{1}$$

with m_p, $\boldsymbol{u_p}$ and ρ_p being respectively mass, velocity vector and density of the particle p; $\boldsymbol{u}$ and ρ air velocity and density; $\boldsymbol{g}$ representing gravity vector, while $\boldsymbol{F}$ encloses additional forces acting on the particle. Saffman lift is included in this term [23], in analogy with similar studies [3]. The equation is expressed in a Lagrangian coordinate system referred to the particle and its integration yields the particle velocity. The first term at RHS of Eq. 1 models drag and depends on the particle's relaxation time τ_r, Eq. 2:

$$\tau_r = \frac{\rho_p d_p^2}{18\mu} \frac{24}{C_d Re} \tag{2}$$

where d_p is the particle diameter, μ air viscosity, *Re* is the relative Reynolds number defined using the particle slip velocity, and C_d the drag coefficient [27]. Turbulence effects on particles due to airflow velocity fluctuations are modelled with a stochastic approach accounting for local turbulent flow characteristics: fluctuating velocity components are randomly defined, and their value is kept constant over an interval of time given by the local characteristic lifetime of the eddies [26]. This approach models the particles turbulent dispersion adding a fluctuating term to the average flow velocity.

2.2 Model validation

To assess the capability of the developed CFD model, a validation test is performed in a fully developed vertical flow, representing a typical configuration investigated by experiments and theoretical treatments on particle deposition. Liu & Agarwal's [28] data are used as validation benchmark as they are acknowledged as a high-fidelity canonical case for turbulent particle deposition [23]. While a circular pipe does not replicate the complex flow separation and recirculation zones typical of insulator sheds, it provides a rigorous test for the model's ability to capture turbulent transport and near-wall phenomena. Validating the solver against this well-characterized flow ensures that the underlying transport mechanisms are correctly implemented before introducing the geometric complexities of insulators. This approach is further necessitated by the current scarcity of high-resolution, open-source experimental data specifically documenting particle dry deposition on electrical insulators [13, 29]. Moreover, physical properties of particles employed in the experimental campaign well overlap with the investigated conditions, Sect. 2.3.2. In addition, a sufficiently wide set of inflow conditions is explored, covering the range of inflow conditions relevant to this work. More in detail, Liu & Agarwal measured deposition rate of aerosol particles in turbulent flows with *Re* = 10'000 and *Re* = 50'000 in a glass pipe with internal diameter d_{IN} =1.27*cm* and length *l*=102*cm*. Aerosol particles used in the experiments are uniform, spherical oil droplets with diameters from 1.4 to 21 μm. Deposition results are reported for a 50.8*cm* deposition section of the deposition pipe. This setup, Fig. 1 (left), has been reconstructed in ANSYS SpaceClaim and the CFD model has been implemented in ANSYS Fluent with the same settings of the model described in Sect. 2.1. Specific measures have been applied in order to provide a fully developed inflow at the inlet, to properly reproduce the experiment conditions. An 800'000-cells computational grid has been constructed to reproduce the inner portion of the modelled deposition pipe, Fig. 1 (right), with a 10-cells prism layer applied at the wall and a combination of hexahedra and polyhedral used for the volume mesh.

The results of the deposition experiments, Fig. 2, are presented in terms of dimensionless particle deposition velocity u_{dep}^+ as a function of dimensionless particle relaxation time τ^+, Eqs. 3 and 4:

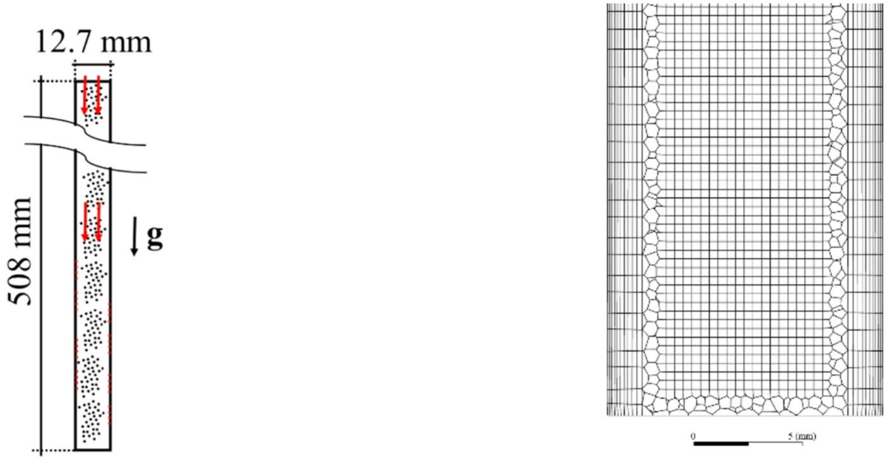

Fig. 1 Left: sketch section of the modelled setup. Right: detail of the computational grid section, with the outlet section at the bottom. The flow direction is top-down

Fig. 2 Dimensionless particle deposition velocity as a function of dimensionless particle relaxation time, comparison of experimental results (empty) and CFD model (solid) predictions for Re = 10’000 (circle) and Re = 50’000 (triangle)

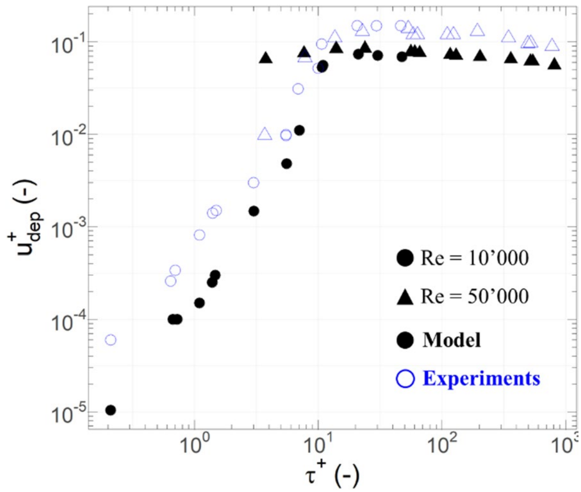

$$u^+_{dep} = \frac{u_{dep}}{u_*} \tag{3}$$

$$\tau^+ = \frac{\tau u_*^2}{\nu} \tag{4}$$

with u_{dep} being the particle deposition velocity, ν the air kinematic viscosity, u_* the flow friction velocity given by Eq. 5 as a function of the wall shear stress τ_w, and τ the particle relaxation time expressed by Eq. 6:

$$u_* = \sqrt{\frac{\tau_w}{\rho}} \tag{5}$$

$$\tau = \frac{\rho_p d_p^2 C_d}{18\mu} \tag{6}$$

Modelled and experimental data are in good agreement, with a Root Mean Square Error *RMSE* < *0.05*. It is then possible to conclude that the CFD model predicts reasonably well the particle deposition velocities across the whole particle diameter range for both measured flow conditions, thus it is considered capable of properly reconstructing the particles deposition process on the insulators surface, as it correctly models relevant phenomena to particles deposition, such as molecular and turbulent diffusion, inertial and gravitational effects.

2.3 Investigated conditions

2.3.1 Geometric model, computational grid and boundary condition settings

A full-scale 3-plates chain of U120B insulators, Fig. 3, has been explicitly reconstructed and enclosed in a 4500 mm long, 2300 mm wide, 2500 mm high domain. The U120B plate has a diameter of 255 mm, the insulators chain vertical spacing is 146 mm. A 3-unit chain configuration was selected following established methodological approaches in the literature [4, 10, 11, 13]. The central insulator was chosen as the reference unit for deposition analysis, thus excluding the end effects typical of the first and last chain elements. In cross-flow conditions, this 3-unit setup is sufficient to capture the representative flow-particle interactions and the quasi-periodic behaviour of longer strings. Under the hypothesis of longitudinal symmetry, half domain has been simulated to optimize computational resources. The resulting computational domain has been discretized with an unstructured grid of 9 million cells, Fig. 4, composed of a hexahedral core portion and a polyhedral region closer to the domain boundaries. A prismatic multi-cell boundary layer has been applied at the walls, consisting of 10 prism layers to accurately treat the near-wall gradients. The resulting area-weighted average y^+ is consistent with the SST *k-ω* model's automatic wall treatment, which ensures numerical accuracy across the viscous sublayer and the buffer region by blending the appropriate wall profiles [26, 30].

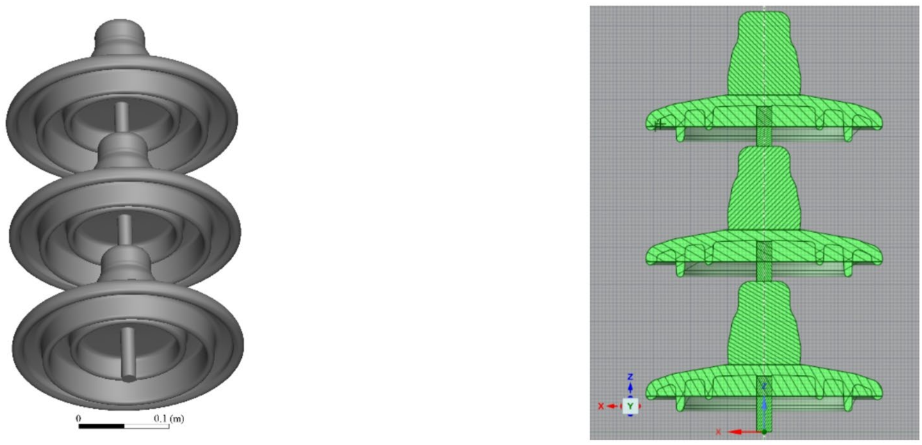

Fig. 3 Modelled 3-plates chain of U120B insulators. Left: 3D view; Right: cross-section

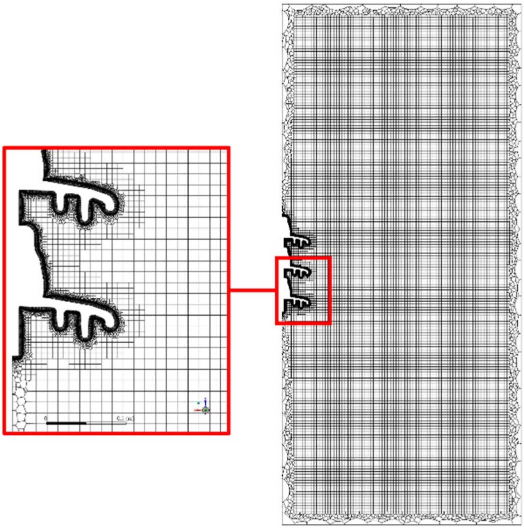

Fig. 4 Details of the computational grid cross-section, highlighting the hexahedral cells for the bulk flow, the prism cells for the wall layer and the polyhedral structures connecting the two regions

Table 1 Wall shear stress approximate relative error for the three grids

Refinement	*N*. of cells	τ_w relative error (%)
Coarse	2.7E+6	4.12
Medium	9.0E+6	3.38
Fine	30.4E+6	–

The grid sensitivity analysis has been performed with a coarser and finer mesh [31], applying a grid refinement factor $r_h \approx 1.5$. Wall shear stress τ_w has been used as reference quantity to assess the non-dependence of the results from the grid refinement, with approximate relative errors below 5%, Table 1. The computed Grid Convergence Index is $GCI_{fine} = 4\%$. 1-D profiles of relevant quantities have been evaluated in different domain regions, highlighting a good agreement between the fine and medium grids. Due to these observations, together with the results of the grid sensitivity analysis, the medium grid has been used throughout the study here presented.

At the domain inlet section, a uniform normal velocity is imposed for the airflow. Particles are injected from random points on the section, with a velocity consistent with the transporting airflow. Turbulence intensity ($I = 5\%$) and viscosity ratio are imposed for the turbulence closure equations. At the outlet section, the operating pressure is imposed at standard atmospheric conditions. The insulators surfaces are treated as rough walls with no-slip conditions; particles deposited on these surfaces are assumed to be retained and no resuspension nor bouncing effects are modelled, in order to simulate the most severe contamination conditions. The remaining external boundaries of the domain (top, bottom, and side) are treated as symmetry planes. This setup avoids the non-physical development of boundary layers at the domain limits and models an unconfined flow, ensuring that the boundaries do not influence the flow field around the insulators chain. The Fluent pressure-based solver is used, with the coupled scheme for pressure-velocity coupling. Second order spatial discretization schemes are applied. Equations residuals and evolution of relevant quantities are monitored to ensure convergence.

2.3.2 Flow conditions

In line with the scope of this work, the parameters space explored by the CFD model has been carefully defined to represent realistic atmospheric conditions and pollutant characteristics in Italy, aiming at meaningful insights on aerosol deposition. Wind speed, ws (m s-1), particle concentration, C (kg m-3) and particle diameter, dp (m), have been chosen as independent variable. Particle density ρp (kg m-3) has been evaluated using a regression curve correlating particle diameter [32]. The values of the independent variables, Table 2, have been defined according to open meteorological and air quality data. More in detail, wind speed data have been retrieved from 30 measurement stations across Italy during the period of 2017-2023. These data were obtained from the Integrated Surface Database (ISD) of NOAA (National Oceanic and Atmospheric Administration) using the "worldmet" R package [33]. The analysis highlighted that ws mostly ranging between 0 and 10 m s-1, with a median around 3 m s-1. The most common wind speed is in the range 0–4 m s-1, with occasional peaks up to 40 m s-1. Aerosol concentration typically varies in the range (0.1; 100) µg m^{-3} over the Italian territory, as reported in previous studies and official air quality assessments [34]. Particle diameter values have been identified by previous measurement campaigns and published studies that characterize aerosol size distributions across various natural and anthropogenic sources [32], selecting the range (0.1–20) µm.

3 Results and discussion

Aerosol deposition is analysed at the top and bottom faces of the central insulator of the 3-units chain simulated, thus excluding peculiar effects of the first and last chain elements.

The flow field around the insulator plays a pivotal role in determining the surface contamination, transporting aerosol particles towards the insulator's surfaces. Significant spatial gradients of the velocity field are observed near the insulator (Fig. 5), flow acceleration is observed close to the upper cap windward side, while low-velocity zones are established at the cap leeward side, under the glass plate, and in the wake region. Intense recirculation and low-velocity regions dominate the bottom surface proximity, as confirmed by the axial velocity contour of Fig. 6. These flow peculiarities are produced by the complex geometry of the plate's bottom surface. At the plate's upper surface, boundary layer separation is observed at the lateral portion, as in [3], see the axial velocity 2D section of Fig. 6 (left). The observed boundary layer separation is caused by an adverse pressure gradient originated in this surface region, as it can be seen in Fig. 6 (center) and Fig. 7 (left), and confirmed by the plot of axial pressure gradient along the axial position, Fig. 7 (right), evaluated at the two distinct transverse locations parallel to the flow direction over the insulator plate, shown as dashed lines in Fig. 7 (left). Adverse pressure gradient and subsequent boundary layer separation is also observed at the leeward region of the insulator's surface.

Table 2 Selected ranges for the model independent variables.

Variable	Min	Max
Wind speed, ws ($m\ s^{-1}$)	0.25	20
Particle concentration, C (μgm^{-3})	0.10	100
Particle diameter, d_p (µm)	0.10	20
Particle density, ρ_p ($kg\ m^{-3}$)	270	2880

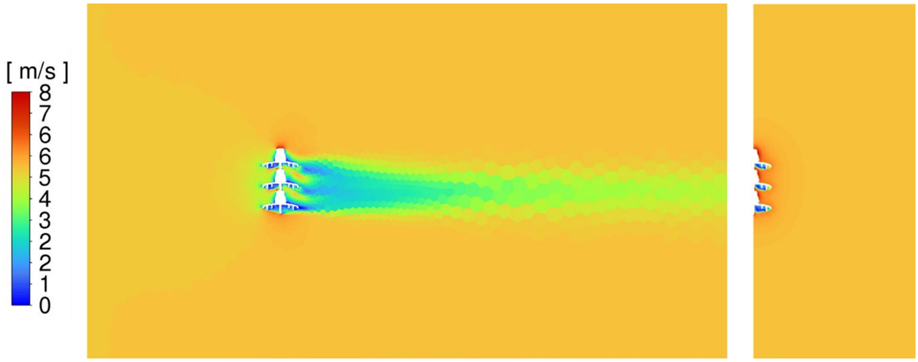

Fig. 5 2D sections of velocity field magnitude (details). Left: geometric symmetry plane; Right: transversal plane. Inlet velocity: 5.1 m s^{-1}. Flow direction: left to right

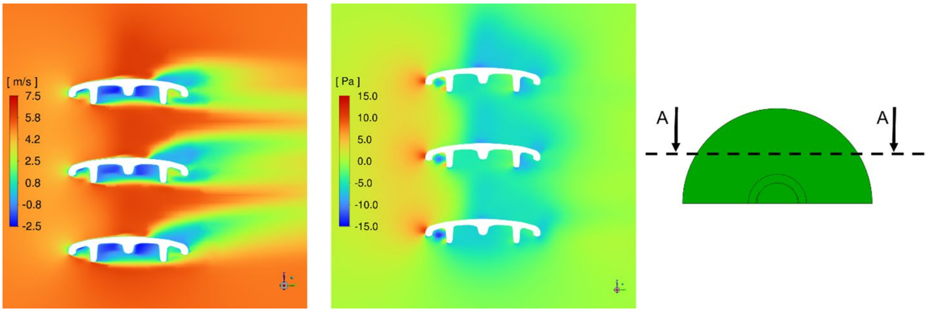

Fig. 6 Details of the axial velocity field 2D section (left) and 2D section of the pressure field relative to the operating pressure (center) on "A-A" cross section (right). Inlet velocity: 5.1 m s^{-1}. Flow direction: left to right

Particle deposition of the insulator's surface exhibits complex behaviours, Fig. 8, with distinct characteristics between the top and bottom surfaces and a pronounced dependence on wind speed and particle diameter. Deposition velocity, u_{dep} ($m\ s^{-1}$), has been chosen as target variable, in line with common approaches in literature [23], and achieving model independence from particle concentration, being obtained by dividing the particle deposition flux by the uniform particle concentration at the domain inlet section, C ($kg\ m^{-3}$), Eq. 7:

$$u_{dep}\left(ms^{-1}\right) = \frac{\dot{Q}_{dep}\left(kgm^{-2}s^{-1}\right)}{C\left(kgm^{-3}\right)} \tag{7}$$

Particle settling velocity is plotted in Fig. 8 for evaluating the contribution of gravitational sedimentation in the deposition mechanism. The settling velocity of spherical particles in air has been calculated verifying Stokes conditions and coherently with the CFD model formulation, following [35]; particle drag coefficients were applied following the correlations of Morsi and Alexander [36], assuring consistency with the CFD model. At very low wind speed ($u < 1\ m\ s^{-1}$), the deposition velocities approach the particles settling veloci-

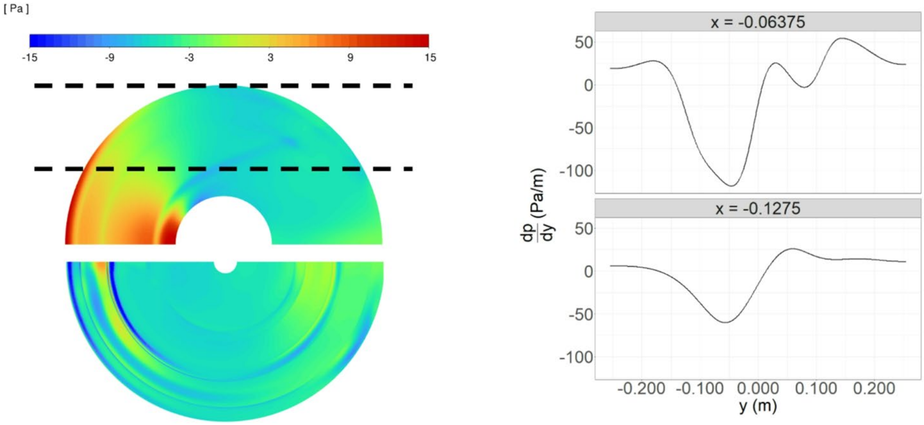

Fig. 7 Left: Relative pressure field at the top and bottom surfaces of the central element of the simulated chain. Inlet velocity: 5.1 m s^{-1}. Flow direction: left to right. Right: Plots of axial pressure gradient (dp/dy) versus axial position y, evaluated at the two distinct transverse locations parallel to the flow direction shown as dashed line onto the pressure field contour. The axis origin is coincident with the plate's geometric center. Pressure is evaluated in reference to operating conditions

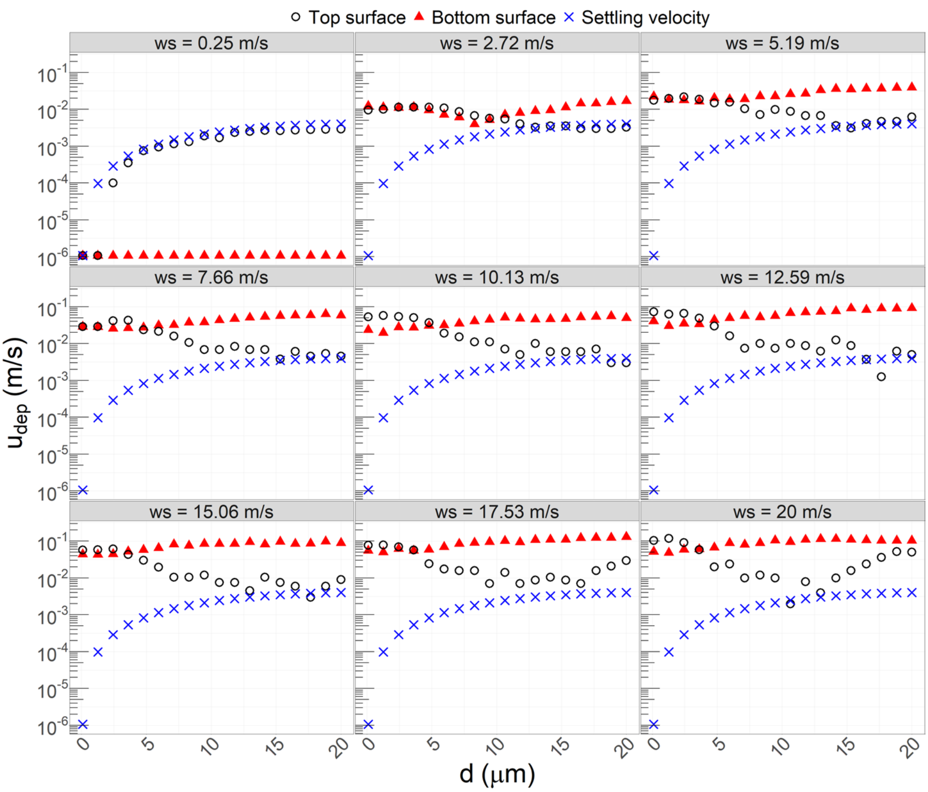

Fig. 8 Deposition velocity u_{dep} (m s^{-1}) onto the top and bottom surfaces of the middle plate for all the investigated conditions. Particles' settling velocity is plotted for comparison

ties, underlining the role of gravitational settling as a relevant deposition mechanism [37]. For higher wind speed, deposition velocities are considerably higher than settling velocities and other deposition mechanisms are relevant. On the upper surface, defined by a smooth, downward-curving profile approximately aligned with the incoming flow, the deposition velocity u_{dep} generally decreases with increasing particle diameter. This trend may be attributed to the combination of streamlines aligned to the deposition surface and elevated inertia of larger particles, resulting in the latter to be less likely to deviate toward and impact the surface. In contrast, finer particles, being more susceptible to turbulent diffusion, are more effectively entrained toward the wall and deposited. The complex geometry at the lower surface promotes the formation of recirculation zones and articulated streamlines configurations. These features facilitate the deposition of larger particles, which are capable of penetrating low-velocity regions and settling onto the surface. Conversely, finer particles are more likely to remain suspended within the recirculating flow, resulting in lower u_{dep} values. These conclusions are clearly supported by u_{dep} trend illustrated in Fig. 8. At the same time more intricate phenomena are observed. A non-monotonic behaviour in u_{dep} is evident for large particles (d > 10 μm ca.) at high wind speed (u > 15 $m\ s^{-1}$) on both surfaces and may be attributed to the substantial momentum of particles under these conditions, which enables them to traverse recirculation zones without significant deviation from their original trajectories, thereby reducing their likelihood of deposition on the lower surface. At the same time, the increase in upper-surface deposition of high-momentum particles may be attributable to their inertial impaction onto the insulator windward section. The presence of adjacent upper and lower plates significantly alters the flow field around the central plate, thereby influencing the deposition dynamics on both the top and bottom surfaces. This inter-plate interaction is consistent with literature findings that emphasize the importance of insulator geometry and mutual aerodynamic interference in shaping local contamination patterns [10, 11, 13].

Particle deposition is confirmed to be a complex phenomenon, given by a combination of several mechanisms. As a representative example, Fig. 9 shows particle impaction locations superimposed onto the pressure distribution for the top surface: impact locations may show the relevance of different mechanisms, such as inertial impaction, turbulent diffusion towards the wall, recirculation zone entrainments.

Our findings provide a more detailed insight into deposition compared to existing literature. While previous studies have often reported contamination in aggregated forms or focused on the macro-distinction between windward and leeward sides [8, 11], the present high-resolution CFD analysis reveals a distinct non-uniform distribution across the insulator's complex profile. Notably, our results identify significant variations between top and bottom surfaces that were not explicitly captured in earlier models [10]. A further element of novelty is the non-monotonic behavior of the deposition velocity (u_{dep}) in relation to particle diameter and wind speed. While several studies suggest more linear or monotonic trends within comparable parameter ranges [4, 8, 10, 11, 13], our model highlights a more complex dependence on particle size and flow conditions. Such insights offer a more precise framework for assessing contaminant accumulation, moving beyond the limitations of aggregated or monotonic deposition models.

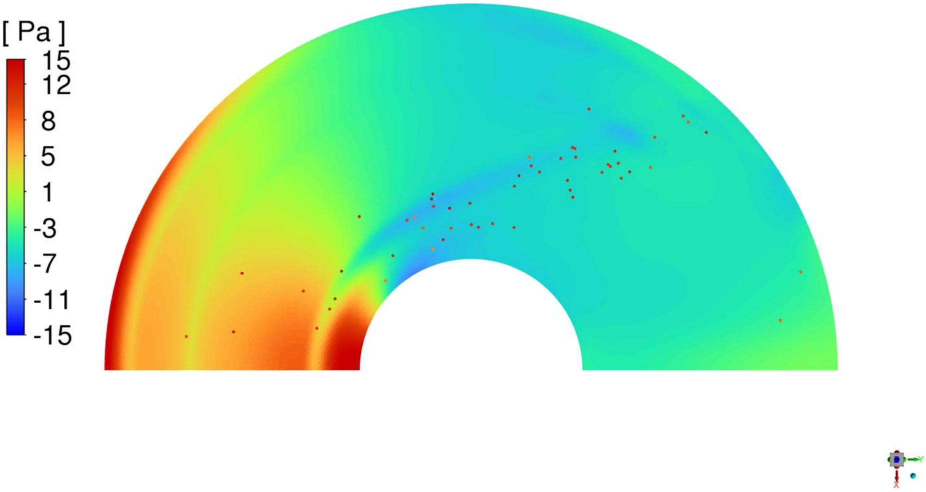

Fig. 9 Particle impaction locations (red marks) superimposed onto the relative pressure distribution on the plate top surface. Inlet velocity: 5.1 m s^{-1}, particle diameter d_p=6.7 μm. Flow direction: left to right. Pressure is evaluated in reference to operating conditions

4 Conclusions

This study presents a validated CFD-based approach for reconstructing dry particulate deposition on a three-unit chain of U120B glass insulators, with a specific focus on fluid dynamics phenomena. The CFD model captures the essential interplay between turbulent flow, particle transport, and deposition mechanisms, accounting for molecular and turbulent diffusion, as well as inertial and gravitational effects across a wide range of particle sizes and wind conditions. Model application shows how insulator shape and local flow patterns influence the spatial distribution of contaminants, highlighting the different deposition behaviours on top and bottom surfaces, the critical roles of wind speed and particle size, and the impact of inter-plate aerodynamic interactions.

These findings move outdoor insulator design and maintenance beyond empirical observations, providing a predictive, physics-based framework, to mitigate contamination. The identified effects of particle size and wind intensity on dry deposition have practical implications for maintenance planning and asset management, supporting strategies to increase power grid resilience to environmental-induced risks. This study addresses dry deposition and does not model electrical and electrostatic effects, with particles modelled as spherical and inert. These choices isolate aerodynamics effects, while excluding processes that may also influence overall contamination.

Future developments may include dedicated experimental investigations to further advance the CFD model development, extension to additional insulator geometries and inclined chain configurations, and expanded representation of surface physics to include particle accumulation and resuspension.

By delivering insights on how geometry-driven flow features interact with particle size and wind intensity on different insulator surfaces, this work provides a solid basis for predictive atmospheric aerosol contamination control and design optimization in overhead power systems.

Acknowledgements This work has been financed by the Research Fund for the Italian Electrical System under the Three-Year Research Plan 2025-2027 (MASE, Decree n.388 of November 6th, 2024), in compliance with the Decree of April 12th, 2024.

Author contributions Conceptualization, N.L.; Methodology, all the authors; Analysis, all the authors; Writing, N.L. and D.T.; Review and editing, all the authors. Scientific supervision, G.P.; Project administration, G.P; All authors have read and agreed to the published version of the manuscript.

Data availability Data availability is subject to Ricerca sul Sistema Energetico S.p.A. approval, provided upon specific request.

Declarations

Competing interests The authors declare no competing interests.

References

1. Hussain MM, Farokhi S, McMeekin SG, Farzaneh M (2017) Mechanism of saline deposition and surface flashover on outdoor insulators near coastal areas part II: impact of various environment stresses. IEEE Trans Dielect Electr Insul 24:1068–1076. https://doi.org/10.1109/TDEI.2017.006386
2. Luciano N, Balzarini A, Toppetti AM, Omodeo P, Pirovano G (2024) A comparative analysis of an aerosol dry deposition microscale model for overhead powerlines insulators. Bull Atmos Sci& Technol 5:17. https://doi.org/10.1007/s42865-024-00080-z
3. Huang Y, Huang X (2020) Flow field distribution around insulator and contamination uneven characteristic of insulator. IET Sci Meas Technol 14:1088–1097. https://doi.org/10.1049/iet-smt.2020.0277
4. Zhao S, Zhang C, Zhang Y, Zhang D (2020) Collision mechanism and deposition characteristics of particles on the catenary insulator surface. Coatings 10:697. https://doi.org/10.3390/coatings10070697
5. Amini MA, Sedighi AR (2014) A new procedure for determination of insulators contamination in electrical distribution networks. Int J Electr Power Energy Syst 61:380–385. https://doi.org/10.1016/j.ijepes.2014.03.034
6. Amicarelli A, Alessandrini S, Agate G, Ferrero E, Pirovano G, Tinarelli GL, Trini Castelli S (2021) A dry deposition scheme for particulate matter coupled with a well-known Lagrangian stochastic model for pollutant dispersion. Environ Fluid Mech 21:433–463. https://doi.org/10.1007/s10652-021-09780-y
7. Farzaneh M, Chisholm WA (2009) Insulators for Icing and Polluted Environments, 1st edn. Wiley, US.
8. Zhang Z, Zhang W, You J, Jiang X, Zhang D, Bi M, Wu B, Wu J (2016) Influence factors in contamination process of XP-160 insulators based on computational fluid mechanics. IET Gen Trans & Distribution 10:4140–4148. https://doi.org/10.1049/iet-gtd.2016.0588
9. Seinfeld JH, Pandis SN (2006) Atmospheric chemistry and physics: from air pollution to climate change, 2nd edn. J. Wiley & sons, New York

10. Qiao X, Zhang Z, Jiang X, Zhang D (2020) Contamination characteristics of typical transmission line insulators by wind tunnel simulation. Electr Power Syst Res 184:106288. https://doi.org/10.1016/j.epsr.2020.106288
11. Zhang Z, Zhang D, Jiang X, Liu X (2014) Study on natural contamination performance of typical types of insulators. IEEE Trans Dielect Electr Insul 21:1901–1909. https://doi.org/10.1109/TDEI.2014.004343
12. Ferrero L, Casati M, Nobili L, D'Angelo L, Rovelli G, Sangiorgi G, Rizzi C, Perrone MG, Sansonetti A, Conti C, Bolzacchini E, Bernardi E, Vassura I (2018) Chemically and size-resolved particulate matter dry deposition on stone and surrogate surfaces inside and outside the low emission zone of Milan: application of a newly developed deposition box. Environ Sci Pollut Res Int 25:9402–9415. https://doi.org/10.1007/s11356-018-1220-2
13. Amicarelli A, Agate G, Ferrero E, Frigerio A (2022) A closed-form solution for the deposition of atmospheric particulate matter on electrical insulators. Environ Fluid Mech 22:891–920. https://doi.org/10.1007/s10652-022-09862-5
14. Zhang Z, You J, Zhao J, Cheng Y, Jiang X, Li Y (2017) Contamination characteristics of disc-suspension insulator of transmission line in wind tunnel. IET Gen Trans Dist 11:1453–1460. https://doi.org/10.1049/iet-gtd.2016.0942
15. Horenstein MN, Melcher JR (1979) Particle contamination of high voltage DC insulators below corona threshold. IEEE Trans Elect Insul EI –14:297–305. https://doi.org/10.1109/TEI.1979.298185
16. Huang Z, Liu Y, Zhang H, Kong Y, Geng J, Liu F, Chen J, Tu Y, Hu S (2024) Comparative study on contamination accumulation characteristics of composite insulators with different shed configurations. IEEE Trans Dielect Electr Insul 31:2731–2740. https://doi.org/10.1109/TDEI.2024.3379158
17. Zhang G, Lan L, Wang Y, Wen X (2022) Simulation study on the pollution accumulation of the porcelain insulator in a wind tunnel under direct-current composite electric field. Electr Power Syst Res 209:108014. https://doi.org/10.1016/j.epsr.2022.108014
18. Görgöz İ, Cebecİ M (2025) Numerical Analysis of Wind-Induced Particle Adhesion on High-Voltage Insulators Using COMSOL Multiphysics. In: 2025 16th International Conference on Electrical and Electronics Engineering (ELECO). IEEE, Istanbul, Turkiye, pp 1–5
19. Ansys, Inc (2024) Fluent, R1
20. CEI (2021) CEI EN IEC 60305
21. Michaelides E, Crowe CT, Schwarzkopf JD (2016) Multiphase Flow Handbook. Taylor & Francis Group, an informa business, UK
22. Prosperetti A, Tryggvason G (2007) Computational Methods for Multiphase Flow. Cambridge University Press, Cambridge
23. Guha A (2008) Transport and deposition of particles in turbulent and laminar flow. Annu Rev Fluid Mech 40:311–341. https://doi.org/10.1146/annurev.fluid.40.111406.102220
24. Lai K, Nazaroff AC WW, (2000) Modeling indoor particle deposition from turbulent flow onto smooth surfaces. J Aerosol Sci 31:463–476. https://doi.org/10.1016/S0021-8502(99)00536-4
25. Bouris D, Triantafyllou AG, Krestou A, Leivaditou E, Skordas J, Konstantinidis E, Kopanidis A, Wang Q (2021) Urban-scale computational fluid dynamics simulations with boundary conditions from similarity theory and a mesoscale model. Energies 14:5624. https://doi.org/10.3390/en14185624
26. Ansys, Inc (2024) ANSYS Fluent Theory Guide 2024 R1
27. Hinds WC (2012) Aerosol Technology: Properties, Behavior, and Measurement of Airborne Particles, 2nd Edition. Wiley-Interscience, New Jersey
28. Liu BYH, Agarwal JK (1974) Experimental observation of aerosol deposition in turbulent flow. J Aerosol Sci 5:145–155. https://doi.org/10.1016/0021-8502(74)90046-9
29. Farmer DK, Boedicker EK, DeBolt HM (2021) Dry deposition of atmospheric aerosols: approaches, observations, and mechanisms. Annu Rev Phys Chem 72:375–397. https://doi.org/10.1146/annurev-physchem-090519-034936
30. Menter FR, Kuntz M, Langtry R Ten years of industrial experience with the SST turbulence model. Heat and Mass Transfer 4(1):625-632.
31. (2008) Procedure for estimation and reporting of uncertainty due to discretization in CFD applications. J Fluids Eng 130. https://doi.org/10.1115/1.2960953
32. Gini I, Balzarini A, Fialdini L, Toppetti AM, Pietrodangelo A, Borelli M (2024) Attività sperimentali a supporto dello sviluppo del sistema modellistico previsionale dei livelli di contaminazione degli isolatori. Ricerca di Sistema, RSE, Milano, p 24012624
33. Carslaw D, Davison J (2025) Worldmet: import surface meteorological data from NOAA Integrated surface database (ISD). https://openair-project.github.io/worldmet/
34. Agresti V, Amicarelli A, Balzarini A, Toppetti AM, Piccoli A, Basla B (2019) Sviluppo del sistema modellistico di qualità dell'aria e primo aggiornamento del caso base di riferimento a scala nazionale. Ricerca di Sistema,, Milano. RSE, n. 19012988

35. Gosman AD, Loannides E (1983) Aspects of computer simulation of liquid-fueled combustors. J Energy 7:482–490. https://doi.org/10.2514/3.62687
36. Morsi SA, Alexander AJ (1972) An investigation of particle trajectories in two-phase flow systems. J Fluid Mech 55:193–208. https://doi.org/10.1017/S0022112072001806
37. Sehmel GA (1980) Particle and gas dry deposition: a review. Atmospheric Environ (1967) 14:983–1011. https://doi.org/10.1016/0004-6981(80)90031-1